INTERNATIONAL JOURNAL OF HYDROGEN ENERGY XXX (2017) 1–9

Available online at www.sciencedirect.com

ScienceDirect

journal homepage: www.elsevier.com/locate/he

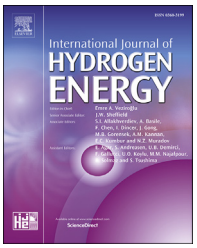

Minimising the ohmic resistance of an alkaline electrolysis cell through effective cell design

Robert Phillips, Adam Edwards, Bertrand Rome, Daniel R. Jones, Charles W. Dunnill[*]

Energy Safety Research Institute, Swansea University, Swansea University Bay Campus, Fabian Way, Swansea, SA1 8EN, UK

ARTICLE INFO

Article history:
Received 5 June 2017
Received in revised form
13 July 2017
Accepted 21 July 2017
Available online xxx

Keywords:
Alkaline electrolysis
Electrochemical impedance spectroscopy
Zero gap
Porous electrodes
Renewable energy storage

ABSTRACT

The efficiency of an alkaline electrolysis cell depends strongly on its internal cell resistance, which becomes the dominant efficiency driver at high current densities. This paper uses Electrochemical Impedance Spectroscopy to decouple the ohmic resistance from the cell voltage, and, for the first time, quantify the reduction in cell resistance achieved by employing a zero gap cell configuration when compared to the conventional approach. A 30% reduction in ohmic resistance is demonstrated for the zero gap cell when compared to a more conventional design with a 2 mm electrode gap (in 1 M NaOH and at standard conditions). The effect on the ohmic resistance of operating parameters, including current density and temperature, is quantified; the zero gap cell outperforms the standard cell at all current densities, particularly above 500 $mA \cdot cm^{-2}$ Furthermore, the effect of electrode morphology on the ohmic resistance is investigated, showing that high surface area foam electrodes permit a lower ohmic resistance than coarser mesh electrodes. These results show that zero gap cell design will allow both low cost and highly efficient alkaline electrolysis, which will become a key technology for short term and inter-seasonal energy storage and accelerate the transition towards a decarbonised society.

Introduction

As intermittent renewable energy generation capacity continues to grow rapidly, energy storage has become a key focal area, essential to assist an efficient transfer towards a decarbonised society. A cost-effective, efficient and scalable technology is crucial to fill this space and facilitate the integration of the booming solar and wind sectors. Energy storage as hydrogen, produced by the electrolysis of water, will be a key player in grid-scale energy storage, as well as playing a vital role in the decarbonisation of transport. This technology allows the buffering of energy supply and demand both in the short term and on inter-seasonal time scales; a key advantage over other methods. Alkaline electrolysis is a mature technology, and systems on the MW scale have been operated for many years [1]. Modern demands on hydrogen production require both low capital costs and high efficiencies, something that modern alkaline electrolysers are looking to address.

Traditional 'finite gap' alkaline electrolysis based on two electrode plates separated by a liquid alkaline electrolyte

* *Corresponding author.*
E-mail address: c.dunnill@swansea.ac.uk (C.W. Dunnill).

http://dx.doi.org/10.1016/j.ijhydene.2017.07.184

suffers from low current densities (<250 mA·cm^{-2}) at low efficiencies (<60%), principally due to high internal resistance losses [2–4]. Other water splitting technologies, most notably Proton Exchange Membrane (PEM) electrolysis, have been developed, and demonstrate higher current densities (>2000 mA·cm^{-2}) at higher efficiencies (>72%) [5–8]. Recent installations on the commercial scale are dominated by PEM technology; however their widespread adoption is limited by the high cost of both the Nafion membrane, and the noble metal catalysts such as platinum or iridium needed because of the acidic environment. Intense development of new catalysts and the availability of a cheap and stable gas separator, together with modern cell design, has led to a resurgence of interest into alkaline electrolysis, with the prospect of both low cost and highly efficient electrolysis being a strong attraction [9–13].

Previous work regarding the optimisation of cell design has been principally based around investigations by Nagai et al., who used DC voltage polarisation data to show that a decrease in electrode gap causes cell voltage reductions at low current densities, and demonstrated the experimental exception to Ohms law at high current densities due to the increase of the electrolyte void fraction from the evolved gas bubbles. Nagai et al. proposed the existence of an optimal gap between electrodes of 2 mm at high current densities (500 mA·cm^{-2}) [14].

LeRoy et al. showed that when gas bubbles are being evolved, the increase of the volume fraction of bubbles between the electrode will increase the electrical resistance of the electrolyte, whilst the effect of electrolyte flow on finite gap cell performance was investigated by Zhang and Zeng as well as Bongenaar-Schlenter, showing electrolyte flow to be key to reducing the effect of gas bubbles, especially at high current densities [15,16]. Zhang investigated cell performance based on the cell polarisation data, which is limited as by using this method the ohmic resistance is not isolated from electrode performance, wheras Bongenaar-Schlenter used a segmented nickel electrode, with multiple reference electrodes to build up a holistic view of the performance inside the cell. Dedigama et al. used Electrochemical Impedance Spectroscopy (EIS) to isolate the ohmic resistance of a PEM electrolyser, and studied the effects of different flow rates and flow regimes, indicating the localised cell heating can be an important factor at low flow rates. No studies on the cell performance have been done for alkaline electrolysis using EIS, which is unique from the PEM setup as the catalyst layer is deposited directly onto the current collector [17–20].

The employment of the zero gap cell design, as discussed recently by Pletcher and Li, looks to push the performance of alkaline cells towards that of PEM whilst maintaining the benefits of cheaper cell materials, and works by compressing two porous electrodes either side of a hydroxide ion conducting membrane or gas separator [2]. This achieves a gap between the two electrodes equal to the thickness of the membrane (≤0.5 mm) rather than (≥2 mm) for the traditional setup (Fig. 1). Zero gap cell design has been discussed by a number of authors [21–24], and its designs demonstrated in an earlier paper [25], although to the best of our knowledge, its benefits over conventional designs are yet to be directly quantified.

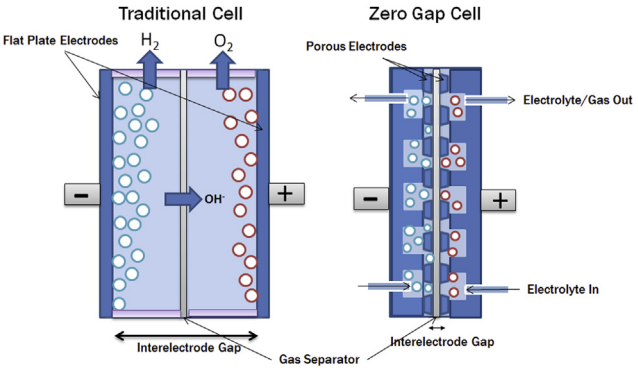

Fig. 1 – Schematic showing the reduction of the inter-electrode gap achieved by employing a zero gap cell design vs the traditional finite gap design.

Many different porous electrode morphologies have been reported in the literature regarding alkaline electrolysers, including perforated plates, expanded mesh, woven mesh and metal foam, although no direct comparisons of the structures has been made [21,22,26]. The effect of the structural properties of current collectors has been investigated for PEM systems, with the pore size shown to effect the ohmic resistance of the cell, as well as its performance at high current densities [27,28].

Information regarding the ohmic resistance of alkaline electrolysis systems is lacking in the literature, with adjustments of design and operating parameters generally investigated only with regards to its effect of cell voltage. This paper quantifies the ohmic resistance savings achieved by employing a zero gap design, as well as demonstrating the effects of current density and electrolyte flow rate on the ohmic resistance of both finite gap and zero gap cell designs. Furthermore, the effect of the electrode morphology on the cell resistance is investigated.

The use of Electrochemical Impedance Spectroscopy (EIS) in this study allows the cell resistance to be decoupled from the overall cell voltage, allowing the effects of cell design to be investigated, without the influence of electrode performance. This is particularly important when making comparisons between setups using different materials, as well as with other setups reported in literature. Current density i, (mA·cm^{-2}) and area specific resistance R, (Ω·cm^2) are used at all times to allow straightforward comparison of data to other systems.

Cell theory

Cell voltage

The overall voltage of an alkaline electrolysis cell is given by

$$E_{Cell} = E_{Rev} + \eta_{Anode} + \eta_{Cathode} + I \times R_{Ohmic} \quad (1)$$

where E_{Rev} is the reversible cell voltage (1.23 V at standard conditions), η_{Anode} is the overpotential at the anode, $\eta_{Cathode}$ the overpotential at the cathode, I the current and R_{Ohmic} the ohmic resistance of the cell.

Please cite this article in press as: Phillips R, et al., Minimising the ohmic resistance of an alkaline electrolysis cell through effective cell design, International Journal of Hydrogen Energy (2017), http://dx.doi.org/10.1016/j.ijhydene.2017.07.184

The motivation to achieve a low cell voltage at useful current densities can be demonstrated using the cell efficiency, which can be expressed as

$$Efficiency = \frac{E_{Rev} \times I \times t}{E_{Cell} \times I \times t} = \frac{E_{Rev}}{E_{Cell}} = \frac{1.23V}{E_{Cell}} \quad (2)$$

Electrocatalyst materials with low overpotentials are much studied [9,29,30], however investigations regarding the ohmic resistance of the cell are scarce, despite its key impact on cell performance.

Note on resistance

The resistance of an electrolysis cell is expressed as

$$R = \frac{\rho_{cell} l}{A} \quad (3)$$

where R is resistance (Ω), A is cross sectional area (cm^2), l thickness of cell (cm), and ρ_{cell} is the specific electrical resistance of the cell (Ω·cm). To allow for easy comparison between setups, area specific electrical resistance R_{asp} is used such that

$$R_{asp} = RA = \rho_{cell} l \quad (4)$$

with units of ($\Omega \cdot cm^2$).

Ohmic resistance

The voltage drop between the electrodes can be expressed using Ohms law

$$V = iR_{Ohmic} \quad (5)$$

where i is the current density in $A \cdot cm^{-2}$, R_{Ohmic} is the area specific resistance of the cell in ($\Omega \cdot cm^2$). When no gas bubbles are being evolved,

$$R_{Ohmic} = R_{Membrane} + R_{Electrolyte} \quad (6)$$

The area specific resistance of the membrane is constant (due to constant thickness and resistivity), and the area specific resistance of the electrolyte is a function of electrolyte resistivity and distance, such that

$$R_{Ohmic} = R_{Membrane} + \rho_{Electrolyte} l \quad (7)$$

Consequently, when the choice of electrolyte concentration is fixed during alkaline electrolysis, R_{Ohmic} varies with l, the distance between the two electrodes.

Electrolyte resistivity

Treating the electrolyte resistivity ($\rho_{electrolyte}$) as a fixed value does not hold true in working conditions; LeRoy et al. showed that when current is flowing, and gas bubbles are being evolved, the increase of the volume fraction of bubbles between the electrode will increase the electrical resistance of the electrolyte [31]. Nagai et al. demonstrated that when the electrode gap is small and the volume fraction is large, the electrical resistance of the electrolyte becomes particularly large, and an optimum distance between electrodes was found to exist at high current densities [14].

The employment of the zero gap design aims to minimise the ohmic resistance by minimising l, the distance between the electrodes, as well as allowing gas bubbles to be released from the backside of the electrodes, reducing the increase in ρ_{cell} due to rise of the void fraction. The ultimate aim of advanced cell design is to eliminate the resistance contribution from the electrolyte, even at high current densities, such that $R_{Ohmic} = R_{Membrane}$.

Effect of gas bubbles

The effect of electrolytic gas bubbles on the cell performance was investigated further by Zeng and Zhang, who modelled the bubble formation on a metal electrode in a stagnant electrolyte, showing the critical diameter of bubble detachment to be a function of buoyancy, expansion force and interfacial tension force, and showing electrolyte concentration to have a key effect [15]. With electrolyte circulation, the additional forces on the gas bubble cause early detachment of the bubbles, and Zeng and Zhang demonstrate a small reduction in the cell voltage when flowing electrolyte is used; attributed to early detachment of the bubbles. The bulk of the resistance was still present and this was attributed to the bubble curtain between the two electrodes. Bongenaar-Schlenter et al. showed that the electrolyte flow rate reduces the cell resistance in a finite gap cell, with large reductions in cell voltage was reported at high current densities ($> 500\ mA \cdot cm^{-2}$), suggesting that the void fraction in the inter-electrode gap being the key factor, and that the effects from the bubble curtain suggested by Zhang could be mitigated [16].

Electrode surface morphology

The electrode morphology can have a synergistic effect on both the overpotentials (η) and the ion transport resistance ($R_{Electrolyte}$) when using porous electrodes. As such, the electrode morphology must be subdivided into the macroscopic structural morphology and the microscopic surface morphology. The overpotential at an electrode is affected by both the intrinsic activity of the catalyst material, and the effective surface area of the electrode. Modifications of electrode surface morphology are made to increase the real electrode surface area; producing active sites such as cracks and crevices which promote the release and capture of electrons [32]. Raney Nickel is a key example, with its excellent catalytic performance when compared to smooth nickel demonstrated by a number of research groups [26,33–36]. This high performance is attributed to its large effective surface area, resulting from its high porosity and nanocrystalline structure. The use of high surface area electrodes with favourable structural morphologies, such as meshes and foams, provide higher surface area substrates than flat plate electrodes; this contributes to a further increase in real surface area, as well as a possible reduction in the ohmic resistance due to smaller ion conduction distances. In this study, the ohmic resistance is decoupled from the overpotentials, but the benefits of employing 3-dimensional electrodes are recognised as being twofold.

Please cite this article in press as: Phillips R, et al., Minimising the ohmic resistance of an alkaline electrolysis cell through effective cell design, International Journal of Hydrogen Energy (2017), http://dx.doi.org/10.1016/j.ijhydene.2017.07.184

Experimental methods

Materials

Stainless steel plates (SS 316, thickness: 1 mm, 3 mm), expanded stainless steel mesh (Dexmet 5 SS 316–050A), woven stainless steel mesh (Mesh Direct (SS 316 #12, #40)), expanded nickel mesh (Dexmet 5 Ni 5–050A), nickel foam (GoodFellow, thickness: 1.6 mm, porosity: 95%) and sodium hydroxide (≥98%, Sigma-Aldrich) were obtained and used as supplied.

Experimental cell design

A square cell was constructed with a surface area of 10 cm^2; spacers and gaskets were fabricated using acrylic and silicone to provide a realistic cell which allowed variation of the distance between electrodes. Grade 316 stainless steel plates were polished using 150, 300 and 600 grit sandpaper, then sonicated for 20 min in acetone and ethanol before being used as electrodes. A Zirfon Perl UTP 500 separator membrane (Agfa) was hydrated for 48 h in 1 M NaOH before use.

The zero gap components are displayed in Fig. 2b; the mesh and foam were cut into 3.15 × 3.15 cm pieces (geometric area 10·cm^2) and degreased by sonication in acetone and ethanol for 20 min each. To remove the oxide layer from the materials, the stainless steel mesh was sonicated in 20% vol. HNO_3 at 40 °C for 10 min, and the nickel mesh/foam was sonicated in 5 M HCl solution at 25 °C for 20 min. All samples were then rinsed in de-ionized water, and dried under a stream of nitrogen. Flow plates were fabricated using 3 mm thick stainless steel plates, with a single channel serpentine flow field etched

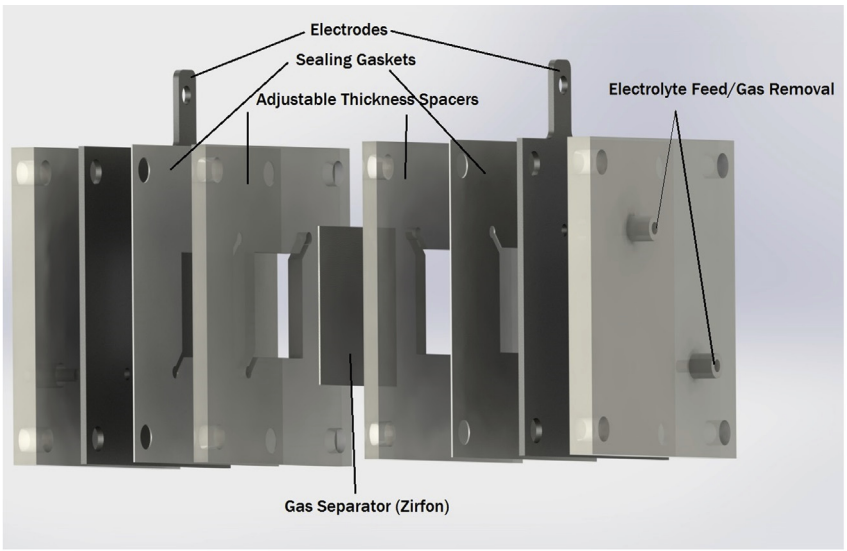

(a) 3d drawing of the cell used, with cell spacers of varying thicknesses to allow the variation of the gap between the electrodes.

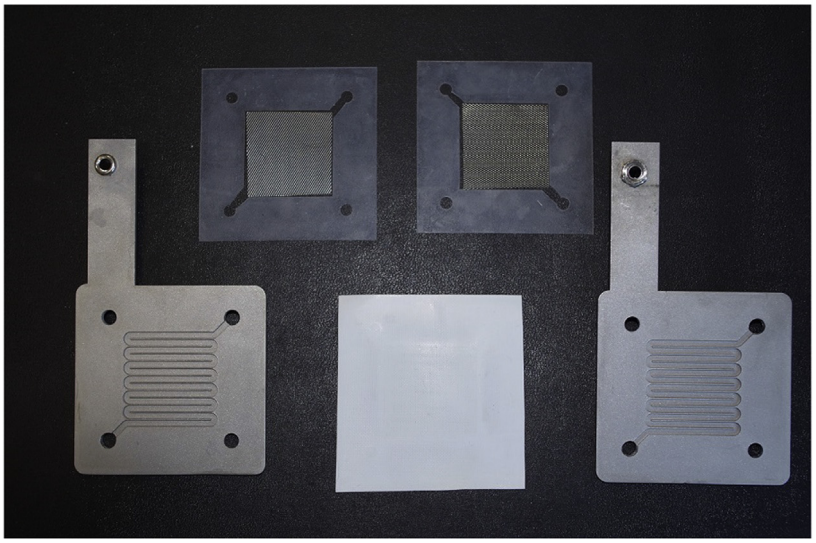

(b) Components for the zero gap cell, including the machined flow field plates, silicone gaskets, mesh electrodes, and Zirfon gas separator.

Fig. 2 – The cell in 2a allows the inter-electrode gap to be varied from 20 to 2 mm, and the zero gap cell in 2b allows this distance to be reduced to the thickness of the gas separator.

Please cite this article in press as: Phillips R, et al., Minimising the ohmic resistance of an alkaline electrolysis cell through effective cell design, International Journal of Hydrogen Energy (2017), http://dx.doi.org/10.1016/j.ijhydene.2017.07.184

to a depth of 1.5 mm; the channels were 2 mm, and the islands 1 mm wide, respectively.

Stainless steel mesh was used to compare the zero gap setup to the finite gap design, and nickel mesh was employed to allow direct comparison of cell polarisation data with nickel foam.

Electrochemical characterisation

All electrochemical characterisation was performed using an Ivium-*n*-Stat multi-channel potentiostat. The ohmic resistance of the cell (R_s) was determined using galvanostatic electrochemical impedance spectroscopy. A signal amplitude of 5% of the applied current and a frequency range (100 kHz–1 Hz). R_s is equated to the impedance at high frequencies, when the phase angle is closest to zero [37]. All measurements were made at 298 ± 2K The cell was allowed to reach equilibrium by applying the desired current density for 300 s before any readings were made.

Scanning Electron Microscopy (SEM) pictures were taken with a Hitachi TM 3030 Plus microscope.

Assembly of the test cell

The test cell was assembled using as-prepared stainless steel plates at either end, as demonstrated in Fig. 2a. Spacers were used either side of the membrane to vary the electrode gap to distances of 2–20 mm, and electrolyte (1 M NaOH) was supplied to the cell via peristaltic pumps, with separate feeds for anodic and cathodic sides to reduce gas mixing in the system. The rate of electrolyte flow is 80 ml·min^{-1} unless stated otherwise, and was calibrated by manual flow rate measurements.

Results and discussion

Cell voltage and efficiency

The effect of *l*, the distance between the electrodes, on the cell voltage is demonstrated in Fig. 3; when operating at 250 mA·cm^{-2}, it is seen to be the dominant contribution to cell voltage. The clear benefit of reducing *l* can be seen, and the further benefit of utilising a zero gap design is demonstrated. The onset potential is the same throughout the experiments at around 1.75 V, well above the reversible potential of water (1.23 V); this is a function of the intrinsic activity of the electrode materials, which are not optimised in this setup, but remain consistent for all designs. The use of appropriate catalysts (such as Ni–Mo for the cathode, Ni–Fe for the anode) can shift this onset potential towards a more desirable value of 1.5 V.

Characterising the ohmic resistance of different cell designs

The ohmic resistance was initially measured at 1 mA·cm^{-2}, so that the influence of evolved bubbles could be neglected. These experimental results show that the internal resistance of the cell varied linearly with the distance between electrodes from 2 to 10 mm; as shown in Fig. 4a, the deviation from this linearity at 20 mm agrees with similar results from Nagai et al.

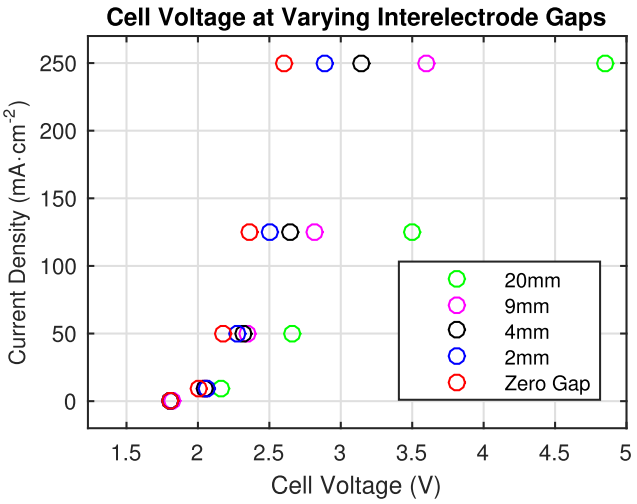

Fig. 3 – Plot comparing the cell voltage at chosen current densities for different cell setups; the increase in cell performance with reduced electrode gap is demonstrated, with the best performance achieved with a zero gap cell configuration.

[14]. The proportionality of the resistance and electrode distance matches well with the theory section, and the figure shows that the lowest internal cell resistance may be achieved when *l* is equal to the thickness of the membrane. The line of best fit is extrapolated backwards to an electrode gap of 0.5 mm, estimating the membrane resistance to be 0.85 Ω·cm^2. The zero gap arrangement achieves the lowest cell resistance, although it is still 42% above the membrane resistance. This difference is principally attributed to the morphology of the porous mesh, such that the transport of ions through solution is not always by the shortest path.

Fig. 4b shows that for all designs, the ohmic resistance of the cell increased with rising current density due to effects of gas bubbles causing an increase in the void fraction of the electrolyte. The ohmic resistances rose by around 0.4 Ω·cm^2 for all electrode gaps with the exception of the zero gap cell, which had a ohmic resistance change of just 0.1 Ω·cm^2. This result shows the clear benefit of employing the zero gap cell setup, and can be attributed to the bubbles being transported away from the mesh electrodes via the backside, minimising the contribution of the bubbles to the inter-electrode void fraction. The cell assembly, including the choice of gasket thickness and cell compression were seen to be important factors in the performance of the zero gap cell; the cell tested here was in an optimised state.

These results show a different approach to cell design can overcome the effects that both Zhang and Bongenaar-Schlenter reported regarding the effects of bubbles. The zero gap arrangement substantially reduces the effect of the bubble curtain, and will require a lower electrolyte flow rate to maintain low ohmic resistance at high current densities when compared to the finite gap cell.

Effect of temperature on cell performance

The effect of temperature on the performance of the zero gap cell was investigated, and the changes in the ohmic resistance

Please cite this article in press as: Phillips R, et al., Minimising the ohmic resistance of an alkaline electrolysis cell through effective cell design, International Journal of Hydrogen Energy (2017), http://dx.doi.org/10.1016/j.ijhydene.2017.07.184

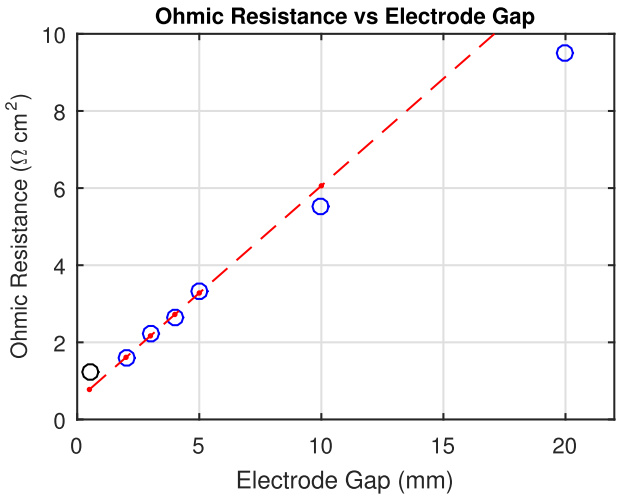

(a) Plot demonstrating the linearity of ohmic resistance with electrode gap up to 10mm, and demonstrated that the lowest cell resistance is achieved using zero gap design, although it is still 42 % larger than the membrane resistance.

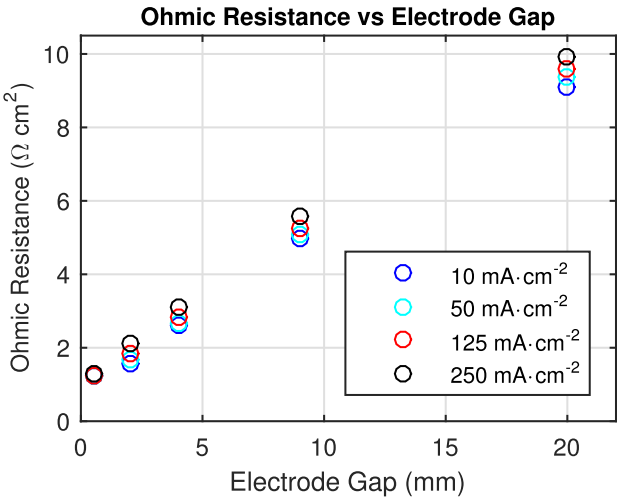

(b) This plot compares the ohmic resistance of different cell configurations at different current densities; the ohmic resistance is seen to increase with current density for all designs, attributed to the increased resistivity of the electrolyte from the gas bubbles. Notably, the rise in ohmic resistance for the zero gap cell is much lower than for the finite gap designs.

Fig. 4 – The effect of electrolyte resistance and high rates of gas evolution on the ohmic resistance of the cell was demonstrated.

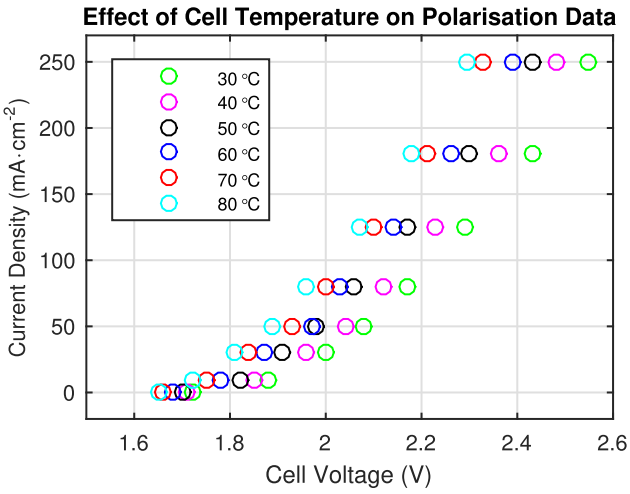

(a) This plot compares the cell polarisation voltage at different cell temperatures, the increase in performance at higher temperatures is attributed to reduced ohmic resistance of the electrolyte filled gas separator

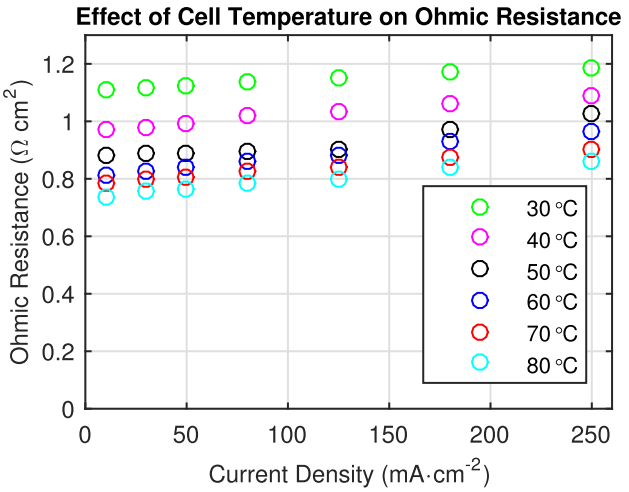

(b) The figure compares the ohmic resistance of the zero gap cell at different temperatures, higher temperatures are clearly favourable due to increase in conductivity of the electrolyte

Fig. 5 – The cell polarisation and ohmic resistance results demonstrate the effect of cell temperature on the performance of the zero gap cell.

of the cell was quantified to extract exact benefits of operating at elevated temperatures. Fig. 5a shows that onset overpotentials were slightly reduced, 1.71 V–1.66 V from 40 °C to 80 °C respectively; this is attributed to favourable electrode kinetics at increased temperatures. A current density of 250 mA·cm^2 was achieved at 2.55, 2.39 and 2.29 V at temperatures of 30, 60 and 80 °C respectively; the reduction in cell voltage is due to both the favourable kinetics at higher temperatures, and the decreased ohmic resistance in the cell. Fig. 5b demonstrates the clear reduction on the ohmic resistance achieved by operating elevated cell temperatures, with a 33% decrease between 30 and 80 °C.

These results offer an insight into the cell performance during the running of a working electrolyser. Optimal operating conditions of 80 °C are widely used, however when the system is starting up/shutting down the stack runs at lower temperatures. Our results demonstrate the key effect that temperature has on the cell performance.

Effect of flow rate of ohmic resistance at different current densities

Fig. 6 shows the reduction of the ohmic resistance by flowing electrolyte for a cell with 2 mm spacing; a 0.4 Ω·cm^2 resistance saving was made by increasing the rate of electrolyte flow from 20 ml·min^{-1} to 80 ml·min^{-1} at 250 mA·cm^{-2}. The ohmic resistance savings become more pronounced at higher current densities. Further resistance savings may have been made by increasing the flow rate further, although the energy required to maintain high flow rates acts to negate the energy saving from the cell resistance. These results are consistent with previous studies, and suggests that the ohmic resistance

Please cite this article in press as: Phillips R, et al., Minimising the ohmic resistance of an alkaline electrolysis cell through effective cell design, International Journal of Hydrogen Energy (2017), http://dx.doi.org/10.1016/j.ijhydene.2017.07.184

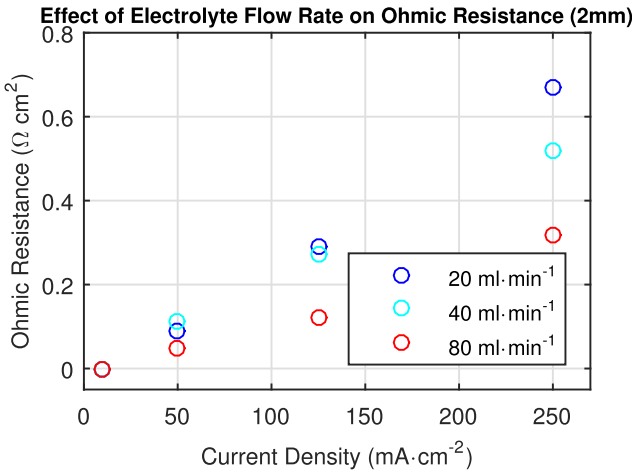

Fig. 6 – Plot comparing the ohmic resistance of the 2 mm gap cell at chosen flow rates; increasing flow rate is shown to reduce the ohmic resistance by removing the bubbles from the electrolyte, reducing the void fraction in the inter-electrode gap.

is governed by the void fraction of the electrolyte between the planar electrodes, rather that the more general suggestion of bubble curtain by Zhang et al. This is evidenced by the sharp reduction in Ohmic resistance associated with flow rate, attributed to the reduced time that each bubble spends in the inter-electrode gap. As the rate of bubble generation is constant, the faster flow rate clears each unit volume of gas in a shorter time, causing a smaller void fraction between the electrodes.

Towards higher current densities

Both the 2 mm and zero gap cells were tested to higher current densities to investigate its effect on the cells' performance. Fig. 7a show that the zero gap cell had a significantly lower voltage at all current densities, even above 500 mA·cm^{-2}; this improvement is likely attributable to the excellent gas management properties of the zero gap cell. This suggestion is supported by 7b, which shows that only small increases in ohmic resistance occurred over the measured range of cell current, even when large amounts of gas evolution was observed. This is consistent with other research showing the large effect of the bubble curtain formed in from of the planar electrode at high current densities; the zero gap cell avoids this issue by forcing the gas bubbles to collect in the flow channels away from the inter-electrode gap. These results demonstrate that the zero gap arrangement overcomes the 'optimal' electrode gap demonstrated by Nagai et al., and sets the modern standard for alkaline electrolyser cell design [14].

Comparison of porous electrodes

A variety of structures, including foams, woven meshes and expanded meshes have been reported as electrode substrates. Nickel foam is widely used as a substrate in studies of OER and HER electrocatalysts due to its exceptionally

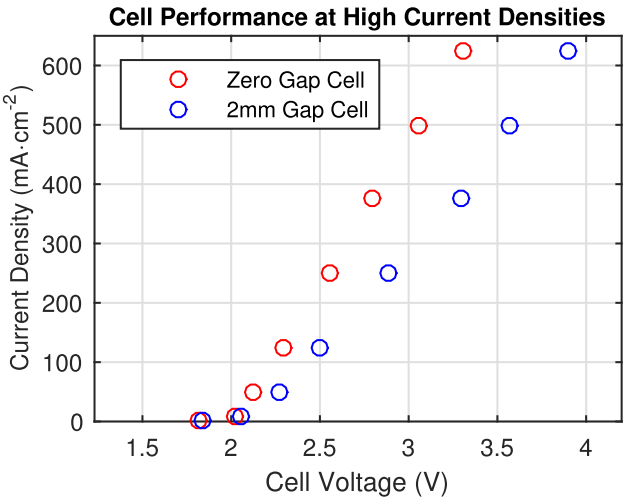

(a) This plot compares the cell polarisation voltage at selected current densities for the 2 mm and zero gap cell's. The data shows that the improved performance from utilising the zero gap arrangement continues, even above 500 mA·cm^{-2}.

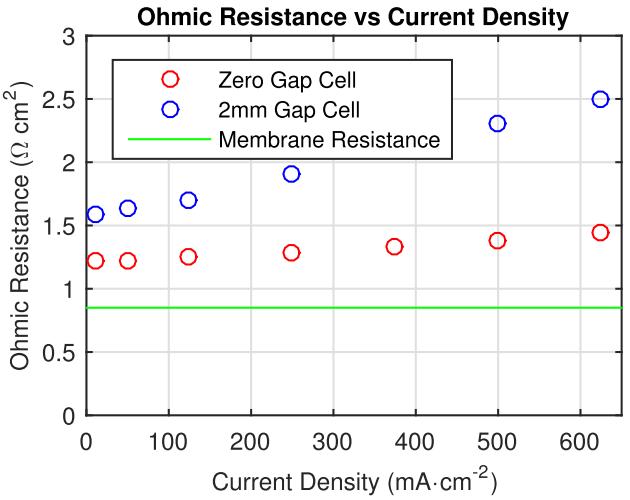

(b) The figure plots the ohmic resistance at chosen current densities for both cells; and shows the ohmic resistance of the 2 mm cell increases faster than the zero gap cell, which has a 18 % increase in ohmic resistance from 0-625 mA·cm^{-2}.

Fig. 7 – The cell polarisation and ohmic resistance results show the benefit of employing a zero gap cell design, even at high current densities.

high surface area vs other substrates. As shown in Fig. 8a, the electrode morphology is seen to affect the ohmic resistance of the cell, with the nickel foam exhibiting the lowest initial ohmic resistance, 2% lower than the expanded mesh. This can be attributed to the lower ion conduction resistance due to the small pores and high surface area of the nickel foam in the immediate vicinity of the gas separator. The coarse woven mesh demonstrates the largest ohmic resistance as expected, due to the large average distance for ion conduction through the electrolyte. These are important results, as it highlights the effect of porous electrode morphology on the ohmic resistance of the cell, a key parameter if alkaline electrolysis is going to be able to compete with the high current densities currently displayed by PEM electrolysers.

Please cite this article in press as: Phillips R, et al., Minimising the ohmic resistance of an alkaline electrolysis cell through effective cell design, International Journal of Hydrogen Energy (2017), http://dx.doi.org/10.1016/j.ijhydene.2017.07.184

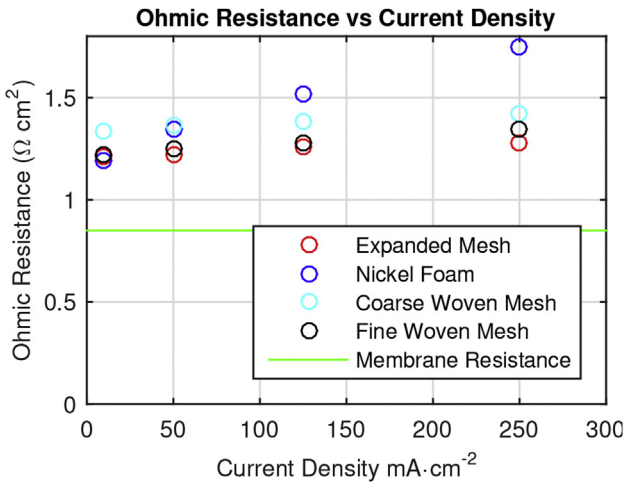

(a) This plot compares the ohmic resistance at chosen current densities for different electrode morphologies. The initial ohmic resistance of the cell with nickel foam as the electrodes is 2 % lower than the next best of the expanded mesh, the coarse woven mesh has the lowest initial value. This is attributed to the reduced distance for ion conduction between the electrodes. The poor performance of the foam cell at high current densities is ascribed to thickness of the nickel foam, causing gas entrapment in the large quantity of pores.

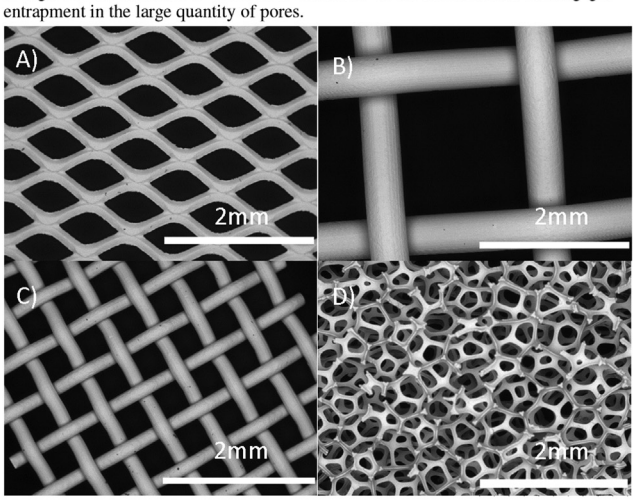

(b) SEM images of the used substrates including A) Expanded mesh, B) Coarse woven mesh (mesh #12), C) Fine woven mesh (mesh #40) and D) Nickel foam (40 pores per inch)

Fig. 8 – The effect of the morphology of various electrodes on the ohmic resistance of the cell, SEM images provide a visual comparison of electrodes used.

When operating at high current densities, the chosen foam became clogged with gas, and showed a steep rise in the cell resistance. This is attributed to both its high porosity and thickness, providing many locations for bubble entrapment, as well as unoptimised operating conditions; further increasing the electrolyte flow rate may mitigate this increase in ohmic resistance. Other research has demonstrated effective integration of nickel foam into laboratory cells [38], indicating that the particular foam tested in this study has some unwanted characteristics. Woven mesh was also found show an increase in the ohmic resistance with current density. The result highlights the need for further research into electrode morphologies, with the criteria focused around providing an electrode with both high surface area, and excellent gas management properties.

Conclusions

Using EIS to decouple the cell resistance and cell voltage, this paper demonstrates the clear benefit of employing zero gap cell design over the conventional finite gap approach, with both a 30% lower initial ohmic resistance as well as smaller resistance increases at high current densities. These benefits are reinforced by the cell polarisation data with higher efficiencies achieved at higher current densities for the zero gap cell. The use of porous mesh electrodes allow easy design, fabrication and assembly of the cell, and the results show that the existence of the optimal electrode gap exhibited by Nagai et al. can be overcome by employing a zero gap cell design.

The influence of the flow rate on the cell resistance is shown, with increased flow rate causing a decrease in ohmic resistance, reinforcing previous studies.

Furthermore, we demonstrate that the use of foam electrodes reduce the ohmic resistance of the cell by 2% when compared to the mesh electrodes used in this study, which exhibits a necessary area of future research focused on the optimisation of electrode morphology on the ohmic resistance of the cell, with the aim of low cell ohmic resistance and good gas management properties.

These results show the potential of zero gap alkaline electrolysis to achieve high current densities currently only associated with the PEM technology; allowing this technology to move towards the key target of low cost and highly efficient electrolysis.

Acknowledgements

Financial support was provided by the Welsh Government Sêr Cymru Programme.

REFERENCES

[1] Paidar M, Fateev V, Bouzek K. Membrane electrolysis history, current status and perspective. Electrochimica Acta 2016;209:737–56.
[2] Pletcher D, Li X. Prospects for alkaline zero gap water electrolysers for hydrogen production. Int J Hydrogen Energy 2011;36(23):15089–104.
[3] Zeng K, Zhang D. Recent progress in alkaline water electrolysis for hydrogen production and applications. Prog Energy Combust Sci 2010;36(3):307–26.
[4] Passas G, Dunnill C. Water splitting test cell for renewable energy storage as hydrogen gas. J Fundam Renew Energy Appl 2015;5(5):188.
[5] Carmo M, Fritz DL, Mergel J, Stolten D. A comprehensive review on pem water electrolysis. Int J Hydrogen Energy 2013;38(12):4901–34.
[6] Laguna-Bercero MA. Recent advances in high temperature electrolysis using solid oxide fuel cells: a review. J Power Sources 2012;203:4–16.
[7] Xu J, Liu G, Li J, Wang X. The electrocatalytic properties of an iro2/sno2 catalyst using sno2 as a support and an assisting reagent for the oxygen evolution reaction. Electrochimica Acta 2012;59:105–12.

Please cite this article in press as: Phillips R, et al., Minimising the ohmic resistance of an alkaline electrolysis cell through effective cell design, International Journal of Hydrogen Energy (2017), http://dx.doi.org/10.1016/j.ijhydene.2017.07.184

[8] Babic U, Suermann M, Bchi FN, Gubler L, Schmidt TJ. Critical review identifying critical gaps for polymer electrolyte water electrolysis development. J Electrochem Soc 2017;164(4):387–99.
[9] Lu X, Zhao C. Electrodeposition of hierarchically structured three-dimensional nickel–iron electrodes for efficient oxygen evolution at high current densities. Nat Commun 2015;6.
[10] Shalom M, Ressnig D, Yang X, Clavel G, Fellinger TP, Antonietti M. Nickel nitride as an efficient electrocatalyst for water splitting. J Mater Chem A 2015;3(15):8171–7.
[11] Prez-Alonso FJ, Adn C, Rojas S, Pea MA, Fierro JLG. Ni/fe electrodes prepared by electrodeposition method over different substrates for oxygen evolution reaction in alkaline medium. Int J Hydrogen Energy 2014;39(10):5204–12.
[12] Li X, Walsh FC, Pletcher D. Nickel based electrocatalysts for oxygen evolution in high current density, alkaline water electrolysers. Phys Chem Chem Phys 2011;13(3):1162–7.
[13] Marini S, Salvi P, Nelli P, Pesenti R, Villa M, Berrettoni M, et al. Advanced alkaline water electrolysis. Electrochimica Acta 2012;82:384–91.
[14] Nagai N, Takeuchi M, Kimura T, Oka T. Existence of optimum space between electrodes on hydrogen production by water electrolysis. Int J Hydrogen Energy 2003;28(1):35–41.
[15] Zhang D, Zeng K. Evaluating the behavior of electrolytic gas bubbles and their effect on the cell voltage in alkaline water electrolysis. Ind Eng Chem Res 2012;51(42):13825–32.
[16] Bongenaar-Schlenter BE, Janssen LJJ, Van Stralen SJD, Barendrecht E. The effect of the gas void distribution on the ohmic resistance during water electrolytes. J Appl Electrochem 1985;15(4):537–48.
[17] Dedigama I, Angeli P, Ayers K, Robinson JB, Shearing PR, Tsaoulidis D, et al. In situ diagnostic techniques for characterisation of polymer electrolyte membrane water electrolysers flow visualisation and electrochemical impedance spectroscopy. Int J Hydrogen Energy 2014;39(9):4468–82.
[18] Dedigama I, Angeli P, van Dijk N, Millichamp J, Tsaoulidis D, Shearing PR, et al. Current density mapping and optical flow visualisation of a polymer electrolyte membrane water electrolyser. J Power Sources 2014;265:97–103.
[19] van der Merwe J, Uren K, van Schoor G, Bessarabov D. Characterisation tools development for pem electrolysers. Int J Hydrogen Energy 2014;39(26):14212–21.
[20] Kobayashi Y, Kosaka K, Yamamoto T, Tachikawa Y, Ito K, Sasaki K. A solid polymer water electrolysis system utilizing natural circulation. Int J Hydrogen Energy 2014;39(29):16263–74.
[21] Kraglund MR, Aili D, Jankova K, Christensen E, Li Q, Jensen JO. Zero-gap alkaline water electrolysis using ion-solvating polymer electrolyte membranes at reduced koh concentrations. J Electrochem Soc 2016;163(11):F3125–31.
[22] Schalenbach M, Tjarks G, Carmo M, Lueke W, Mueller M, Stolten D. Acidic or alkaline? towards a new perspective on the efficiency of water electrolysis. J Electrochem Soc 2016;163(11):F3197–208.
[23] Chatzichristodoulou C, Allebrod F, Mogensen MB. High temperature alkaline electrolysis cells with metal foam based gas diffusion electrodes. J Electrochem Soc 2016;163(11):3036–40.
[24] Vincent I, Kruger A, Bessarabov D. Development of efficient membrane electrode assembly for low cost hydrogen production by anion exchange membrane electrolysis. Int J Hydrogen Energy 2017;42(16):10752–61.
[25] Phillips R, Dunnill C. Zero gap alkaline electrolysis cell design for renewable energy storage as hydrogen gas. RSC Adv 2016;6(102):100643–51.
[26] Pletcher D, Li X, Wang S. A comparison of cathodes for zero gap alkaline water electrolysers for hydrogen production. Int J Hydrogen Energy 2012;37(9):7429–35.
[27] Ito H, Maeda T, Nakano A, Hwang CM, Ishida M, Kato A, et al. Experimental study on porous current collectors of pem electrolyzers. Int J Hydrogen Energy 2012;37(9):7418–28.
[28] Ito H, Maeda T, Nakano A, Kato A, Yoshida T. Influence of pore structural properties of current collectors on the performance of proton exchange membrane electrolyzer. Electrochimica Acta 2013;100:242–8.
[29] Gong M, Dai H. A mini review of nife-based materials as highly active oxygen evolution reaction electrocatalysts. Nano Res 2015;8(1):23–39.
[30] Xiao L, Zhang S, Pan J, Yang C, He M, Zhuang L, et al. First implementation of alkaline polymer electrolyte water electrolysis working only with pure water. Energy Environ Sci 2012;5(7):7869–71.
[31] LeRoy RL, Janjua MBI, Renaud R, Leuenberger U. Analysis of time variation effects in water electrolyzers. J Electrochem Soc 1979;126(10):1674–82.
[32] Zeng K, Zhang D. Evaluating the effect of surface modifications on Ni based electrodes for alkaline water electrolysis. Fuel 2014;116:692–8. http://dx.doi.org/10.1016/j.fuel.2013.08.070.
[33] Herraiz-Cardona I, Gonzlez-Buch C, Valero-Vidal C, Ortega E, Prez-Herranz V. Co-modification of ni-based type raney electrodeposits for hydrogen evolution reaction in alkaline media. J Power Sources 2013;240:698–704.
[34] Herraiz-Cardona I, Ortega E, Antn JG, Prez-Herranz V. Assessment of the roughness factor effect and the intrinsic catalytic activity for hydrogen evolution reaction on ni-based electrodeposits. Int J Hydrogen Energy 2011;36.
[35] Dong H, Lei T, He Y, Xu N, Huang B, Liu CT. Electrochemical performance of porous ni3al electrodes for hydrogen evolution reaction. Int J Hydrogen Energy 2011;36(19):12112–20.
[36] Schiller G, Henne R, Borck V. Vacuum plasma spraying of high-performance electrodes for alkaline water electrolysis. J Therm Spray Technol 1995;4(2):185–94.
[37] Stevens MB, Enman LJ, Batchellor AS, Cosby MR, Vise AE, Trang CDM, et al. Measurement techniques for the study of thin film heterogeneous water oxidation electrocatalysts. Chem Mater 2017;29(1):120–40.
[38] Kim J-H, Lee J-N, Yoo C-Y, Lee K-B, Lee W-M. Low-cost and energy-efficient asymmetric nickel electrode for alkaline water electrolysis. Int J Hydrogen Energy 2015;40(34):10720–5.

Please cite this article in press as: Phillips R, et al., Minimising the ohmic resistance of an alkaline electrolysis cell through effective cell design, International Journal of Hydrogen Energy (2017), http://dx.doi.org/10.1016/j.ijhydene.2017.07.184